Interannual similarity and variation in seasonal circulation of Mars' atmospheric Ar as seen by the Gamma Ray Spectrometer on Mars Odyssey

A.L. Sprague, W.V. Boynton, François Forget, Y. Lian, M. Richardson, R. Starr, A.E. Metzger, D. Hamara, T. Economou

Interannual similarity and variation in seasonal circulation of Mars' atmospheric Ar as seen by the Gamma Ray Spectrometer on Mars Odyssey

Ann L. Sprague,[1] William V. Boynton,[1] Francois Forget,[2] Yuan Lian,[3] Mark Richardson,[3] Richard Starr,[4] Albert E. Metzger,[5] David Hamara,[1] and Thanasis Economou[6]

Received 31 May 2011; revised 22 February 2012; accepted 22 February 2012; published 20 April 2012.

[1] More than 3 Mars' years (MY) of atmospheric argon (Ar) measurements are used to study annual and seasonal variations in atmospheric transport and mixing. Data are obtained over the period 20 May 2002 to 4 May 2008 by the Gamma Subsystem (GS) of the Gamma Ray Spectrometer (GRS) on the Mars Odyssey spacecraft in orbit around Mars. Here we augment previous studies of Mars' Ar in which strong seasonal variations were observed and horizontal meridional mixing coefficients for the southern hemisphere were computed. Comparison of year-to-year seasonal abundance shows strong similarity but also some short-period ($\sim$15°–30° L_s) and interannual variations. Evidence for short periods of strong eddy transport is exhibited during autumn and winter. The seasonal change in Ar concentration for southern latitudes is relatively gradual and well defined, but seasonal changes at high northern latitudes are chaotic and indicate that atmospheric disturbance is ubiquitous. Major topographic landforms (Elysium, Tharsis, Noachis Terra, Hellas) apparently have little control over seasonal Ar concentration at the spatial resolution of the GRS data set. Some indication of local enhanced Ar concentration is present from 30°N to 60°N for the Hellas and Tharsis sectors in late winter and early spring. The data show some significant (3σ) differences between MY 26 and MY 27 in geographical sectors that are likely produced by local weather. The GS data do not show seasonal variation of Ar at equatorial and low-latitude zones, in contrast to those from the Alpha Particle X-ray Spectrometer (APXS) measurements from the Mars Exploration Rovers.

Citation: Sprague, A. L., W. V. Boynton, F. Forget, Y. Lian, M. Richardson, R. Starr, A. E. Metzger, D. Hamara, and T. Economou (2012), Interannual similarity and variation in seasonal circulation of Mars' atmospheric Ar as seen by the Gamma Ray Spectrometer on Mars Odyssey, *J. Geophys. Res.*, *117*, E04005, doi:10.1029/2011JE003873.

1. Introduction

[2] The argon (Ar) mixing ratio in Mars' atmosphere was first measured by the instruments on the Viking Lander 2 (VL2) (the VL1 measurement was considered less reliable), and found to be 0.016 by volume during northern summer at 48°N latitude, 134°E. longitude, at L_s = $\sim$135°. This value has been accepted as the standard for the Mars atmosphere to date [*Owen et al.*, 1977].

[3] Other measurements of Ar in Mars' atmosphere are those made by the Gamma Subsystem (GS) of the suite of three instruments comprising the Gamma Ray Spectrometer (GRS) on the 2001 Mars Odyssey spacecraft [*Boynton et al.*, 2004]. The GS integrates γ-ray line emission at 1294 keV generated by the decay of ^{41}Ar created when a thermal neutron is captured by ^{40}Ar in Mars' atmosphere. Details of measurements made during MY 26 and the beginning of MY 27 are thoroughly discussed by *Sprague et al.* [2004] and *Sprague et al.* [2007] (hereafter referred to as S2004 and S2007, respectively). An exhaustive account of data collection, analysis, and calibration is provided by S2007 where the interested reader may find the details. As presented by S2004 and S2007, Ar concentration was found to change with season and latitude. At high southern latitude, the Ar abundance increased steadily through southern autumn and early winter until it reached a factor of seven or so greater than the Viking value. At about L_s = 120°, an abrupt decrease continued until late spring when it fell below the Viking value and then increased slightly during southern

[1]Lunar and Planetary Laboratory, University of Arizona, Tucson, Arizona, USA.
[2]Laboratoire de Météorologie Dynamique, CNRS, Université Pierre et Marie Curie, Paris, France.
[3]Ashima Research, Pasadena, California, USA.
[4]Department of Physics, Catholic University, Washington, D. C., USA.
[5]Jet Propulsion Laboratory, Pasadena, California, USA.
[6]Laboratory for Astrophysics and Space Research, University of Chicago, Chicago, Illinois, USA.

0148-0227/12/2011JE003873

summer. This behavior is attributed to the accumulation of Ar in the atmosphere at high latitudes as CO_2 freezes out on to the surface. Eventually (at about $L_s = 120°$) the Ar concentration causes a steep meridional gradient that is relieved by eddy mixing toward the equator. At about the same time the effects of dilution by CO_2 subliming from the perimeter of the cap during winter and early spring contribute to the lowering of the Ar concentration. The same analyses recording the large concentrations of Ar at high latitudes in southern winter found that at high northern latitudes in northern winter the accumulation of Ar is less well defined and the mixing ratio underwent fluctuations on times scales of 15° to 45° of L_s. Peaks in Ar abundance reached a factor of 3 greater than the Viking value as predicted by simple advection models.

[4] Since N_2 and Ar are strong thermal neutron absorbers, the neutron spectrometer (NS) was sensitive to the total column of Ar and N_2 during the Odyssey mission. A detailed characterization of Mars' seasonal caps and measurement of the seasonal concentration of noncondensables (N_2 + Ar) in high southern latitudes for MY 26 is given by *Prettyman et al.* [2009] (hereafter referred to as P2009). Results of that study show a strong similarity of noncondensable abundance fluctuations during autumn and winter to those obtained for Ar alone by the gamma ray instrument and described by S2004. The N_2 enhancement factor generally tracks that of the Ar enhancement factor but has higher values in late spring and summer between $L_s \sim 240°$ and $L_s \sim 360°$ (see Figure 8 of P2009). The Alpha Particle X-ray Spectrometer (APXS) on board the Mars Exploration Rovers (MER) also measured atmospheric Ar close to the ground and at equatorial and low latitudes for MYs 27, 28 and 29 [*Arvidson et al.*, 2011]. Measurements give seasonal and interannual variations associated with the subliming of the seasonal CO_2 polar caps. More discussion about these matters will follow.

[5] Another interesting source of information about the behavior of noncondensable gases has been provided by mapping the column abundance of CO in the Martian atmosphere [cf. *Encrenaz et al.*, 2006; *Billebaud et al.*, 2009]. Although it is not as inert as Ar or N_2, CO is a long-lived noncondensable species which is thus assumed to follow the same seasonal evolution as these gases. *Krasnopolsky* [2003] found a systematic trend at $L_s = 112°$ (early southern winter) for CO to have a higher mixing ratio at higher southern latitudes than northern. Also, *Smith et al.* [2009, Figures 10 and 11] show CO concentrations that are lower than average values for both southern and winter summers, following a similar trend as that observed for Ar.

2. The Ar Concentrations for MYs 26, 27, 28, and a Bit of 29

[6] Mars' atmospheric Ar abundance measured by the GS spanning nearly 3 Mars' years has been calculated for this paper in three separate binning arrangements. In section 2.2 we present the entire data set in 15° increments in L_s and circumplanet zonal bands 15° in latitude. This is similar to that of previous work [S2004; S2007] that also shows 360° longitude by 15° latitude "zonal averages" for 15° increments in L_s. All data have been uniformly processed using the same line fitting procedures and electronic binning computer codes. The binning scheme provides a good look at both seasonal and latitude variations for zonal averages of Ar concentration and permits a look at global meridional circulation. Section 2.3 examines an especially chosen data subset with a shorter seasonal binning of 10° L_s to permit a closer look at seasonal fluctuation in data that indicate especially unusual meridional transport. Section 2.4 focuses on meridional averages over distinct topographic regions. Data are binned in four longitude sectors of 90° each. They were chosen to encompass four different topographical regions on Mars' surface: Elysium (120°E to 210°E), Tharsis (210°E to 300°E), Noachis Terra (300°E to 30°E), and Hellas (30°E to 120°E). This partitioning permits a study of the effect of topography on meridional mixing. In section 4 we discuss uncertainties and limitations of the GS data set and its analysis. In section 5 we briefly discuss the potential for Ar data to serve as a standard against which to fine tune future general circulation models. A brief summary and conclusions follow in section 6. Electronic auxiliary materials to this manuscript include GS data for zonal averages in 15° latitude increments and 90° longitude topographic sectors in latitude increments of 30°.[1]

2.1. Complete Gamma Ray Ar Data Set

[7] More than 3 Mars' years of atmospheric argon (Ar) measurements are used to study annual and seasonal variations in atmospheric transport and mixing. Data are obtained over the period 20 May 2002 to 4 May 2008 (MY 26 to MY 28 and 60° of L_s in MY 29) by the Gamma Subsystem (GS) of the Gamma Ray Spectrometer (GRS) on the Mars Odyssey spacecraft in orbit around Mars. This greatly extends the previous measurements: (1) a detailed analysis of Ar concentrations and mixing for MY 26 and part of MY 27 [S2004; S2007], (2) CO_2 depth, N_2 and Ar concentration for MY 26 from a thorough analysis of the Neutron Spectrometer (NS) subsystem of the GRS, also on Mars Odyssey [P2009], and (3) equatorial and low-latitude seasonal Ar variations measured in the surface/atmosphere boundary layer by the APXS [*Economou and Pierrehumbert*, 2010].

2.2. Quantifying Mars' Atmospheric Argon

[8] The absolute calibration method for the extended Ar data set in this paper is the same as that used previously. This is justified because the same instrument operated continuously in the same orbit and no important changes were made in any method of data retrieval, storage, or reduction. Briefly stated, we compute the mass of Ar in the average column of Mars' atmosphere at and around the calibration region of Viking Lander 2 (VL2) by multiplying the estimated atmospheric thickness of a region about the size of the GS footprint as computed using the NASA Ames Research Center (ARC) GCM (version 1.7.3 [*Haberle et al.*, 1993]) by the VL2 mass mixing ratio (0.0145). The grid point (finite difference) numerical model for Mars' atmosphere was originally derived from a terrestrial GCM [*Leovy and Mintz*, 1969]. Several subsequent developments have included [*Pollack et al.*, 1990; *Murphy et al.*, 1995; *Suarez and Takacs*, 1995; *Haberle et al.*, 1999, 2003]. Details of the grid structure, spatial resolution, and physical parameters can be found in the references given, or specifically for our Ar analysis of S2007.

[1] Auxiliary materials are available at ftp://ftp.agu.org/apend/je/2011je003873.

Because Mars has significant topography and strong seasonal changes in atmospheric pressure (mass column abundance) we use atmospheric modeling to generate a standard Mars atmosphere with a constant Ar mass mixing ratio. To correct for the attenuation of 1294 keV γ rays by the atmosphere itself, we use a combination of the NASA ARC GCM with a model of the ratio of 1294 keV γ rays at the spacecraft to thermal neutrons below the spacecraft for many atmospheric thicknesses. As in our previous work, we use the Monte Carlo N-Particle extended (MCNPX) computer code designed specifically to understand neutron production and transport in planetary regoliths [*Waters*, 1999; *Prettyman et al.*, 2004; S2007]. The functional dependence and the correction process are described in detail by S2007 for the interested reader.

2.3. Homogeneous Ar Distribution Model, Enhancement Factors, and Ar Concentration

[9] As with our previous work, we assume Ar is well mixed with altitude and model the attenuation and production of 1294 keV γ line emission using the same linear relationship derived with MCNPX and shown in Figure 5 of S2007. With the relationship for attenuation and production we create a model for all seasons and latitude bins of the equivalent Ar/Ti ratios that would be expected to be measured by the GRS at the GS if Ar in Mars' atmosphere were well mixed over the present topography and had a constant mass mixing ratio of 0.0145. We call this model the *homogeneous Ar distribution model.* As in our previous analyses, this model is used as our standard comparison to the data. A ratio of the actual GS data to this model gives the relative abundance of Ar for the regions and seasons of interest. Because southern winter Ar abundances are much larger than those of the homogeneous Ar distribution model, we call the ratios to the homogeneous Ar distribution model "enhancement factors" even though, at some locations, seasons, and short periods of 15° or so increments of L_s the "enhancement factor" is less than unity.

[10] In many cases it is more convenient to study the Ar abundance as the % concentration in the atmospheric column. In our analyses, the percent concentration is defined as the enhancement factor multiplied by the VL2 mass mixing ratio expressed as a percent of the total column of atmosphere computed by the GCM for the season and location under consideration.

2.4. Model Estimates of Atmospheric Thicknesses

[11] For the zonal averages and the longitude sector model homogeneous atmosphere described in detail in section 3 we used the surface pressure predictor provided with the Mars Climate Database Version 4 [*Forget et al.*, 2007a], as described by *Forget et al*. [2007b, section 4.2]. This tool provides the best possible estimation of the surface pressure by interpolating the reference pressure measured by VL 1 using a high-resolution topography map from MOLA and taking into account the horizontal pressure variations resulting from atmospheric dynamics and the thermal structure using atmospheric simulations from the Laboratoire de Météorologie Dynamique (LMD) General Circulation Model (GCM) [*Forget et al.*, 1999]. At first this may appear to be an inconsistent procedure to use the NASA ARC GCM model atmosphere output for the calibration and then switch to the LMD pressure predictor for the sector model atmosphere and computation of the Ar enhancement factors and concentrations. However, we believe it does not present any increased uncertainty into the analysis but rather, it improves the reliability of the results. This tool was recently able to accurately predict the pressure measurements obtained by the Phoenix lander on Mars' surface in 2008. Thus, although the GS measurements were performed more than 20 Earth years after the VL 1 measurements, it is likely that the global pressure has not significantly drifted. Moreover, outside years with global dust storms, the year-to-year interanual variability is expected to be small, notably in comparison with the day-to-day variability induced by baroclinic years. A small difference in the spatially averaged midlatitude column abundance used in the GS absolute calibration exists between the NASA ARC and the LMD pressure predictor (16.03 g/cm^2 $\pm$ 2.4 g/cm^2 versus 15.71 g/cm^2 $\pm$ 2.3 g/cm^2, respectively, a 2.3% difference. For the sake of consistency in comparisons between the published Ar data sets, we have kept the calibration factor constant in spite of this difference.

3. Ar Concentration

3.1. Ar Concentration in Zonal Averages in 15° Latitude Increments

[12] The GS zonal average Ar concentrations for northern latitudes over all seasons for MYs 26, 27, 28, and 60° of L_s of MY 29 are plotted in Figure 1. To minimize noise and maximize the signal in the equatorial and midlatitude region (0° to 45°N and 0° to 45°S), the so-called "belly band," we have averaged three latitude increments (0° to 15°, 15° to 30° and 30° to 45°) for both the north and south hemispheres. This is in contrast to S2007, who presented individual 15° latitude increments for all latitudes, even equatorial and midlatitudes where the uncertainty in the data was too great to permit diagnostic comparisons. It is clear from comparison of the northern hemisphere data (Figure 1, right) to that of the southern (Figure 1, left) from MY 26 through MY 28 in Figure 1 that the seasonal behavior of Ar concentration is grossly similar from year to year with a steady increase at the highest latitudes in autumn and early winter followed by a steady decline in late winter and spring, especially for the southern hemisphere. This seasonal trend and other differences known to exist between the north and south polar regions such as cloud frequency, aerosol size and distribution [*Colaprete et al.*, 2003] and atmospheric wave activity [*Hollingsworth and Barnes*, 1996] have been previously discussed [S2007]. What has not been previously discussed with respect to northern variability is the dramatic sublimation of CO_2 frost in late fall and early winter inferred from data obtained from the Mars Orbiter Laser Altimeter (MOLA) on Mars Global Surveyor (MGS). *D. E. Smith et al.* [2001] describe an unexpected period of CO_2 sublimation during late autumn in the northern hemisphere coincident with southern hemisphere dust storms. Alternative explanations are wind dispersion of the CO_2 frost or compaction of CO_2 ice thickness or density. Based on our perception of the chaotic nature of the northern Ar enhancement we favor sporadic dilution by sublimation or eddy disturbances causing meridional migration of Ar toward the equator. Regarding the equatorial and low-latitude regions shown in Figure 1, *Spiga et al.* [2011] point out that the active convective boundary layer rises up to 10 km

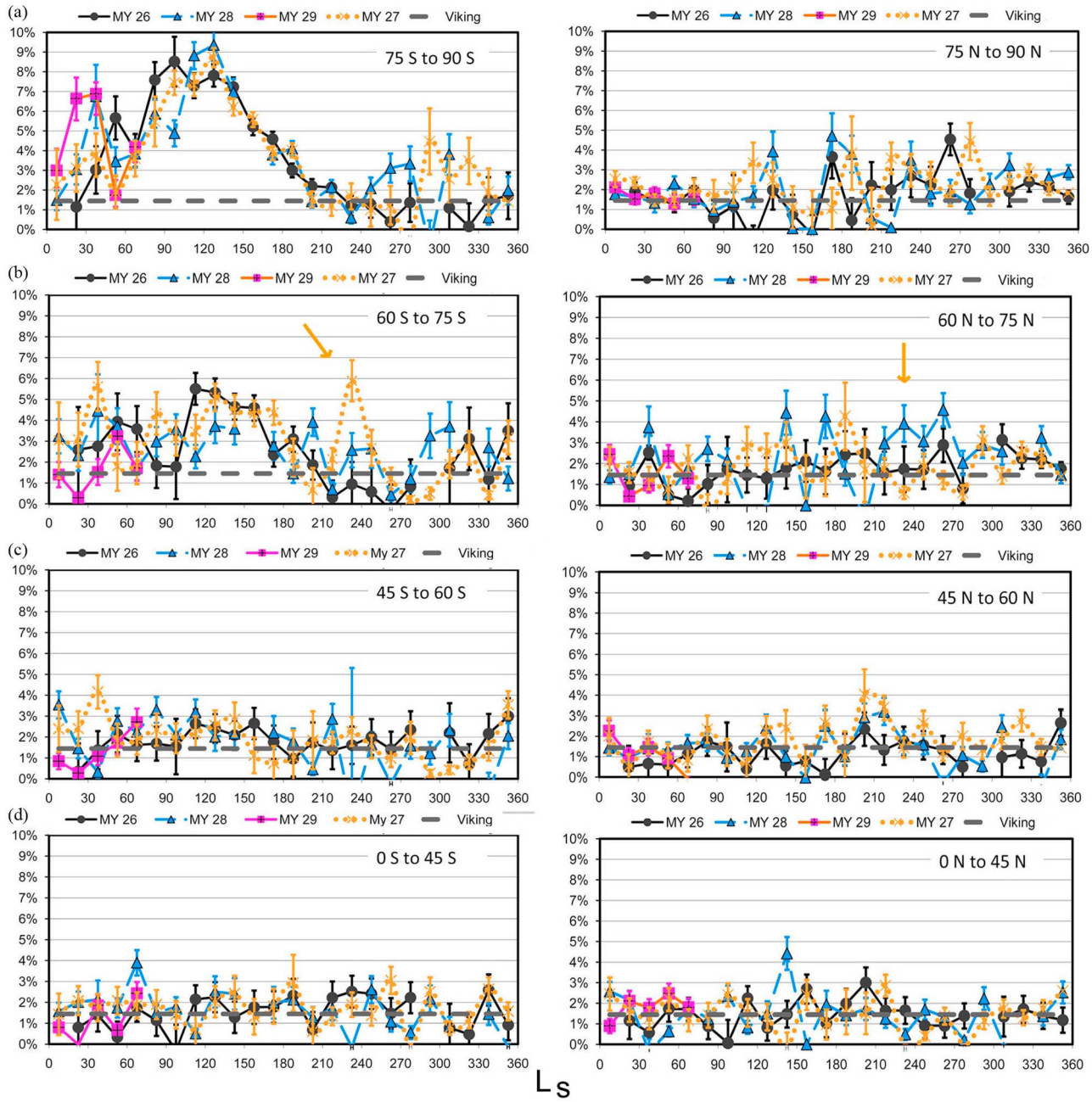

Figure 1. Latitudes (a) 75°S to 90°S, (b) 60°S to 75°S, (c) 45°S to 60°S and (d) 0° to 45°S. (left) Seasonal Ar behavior in southern hemisphere zonal averages for 3 full consecutive Mars' years and the next southern autumn. (right) Seasonal Ar behavior in northern hemisphere zonal averages for Mars' years 26, 27, 28 and five seasons of MY 29. One σ error bars based only on counting statistics are shown. These error bars are shown to be consistent with the scatter in the data at low latitudes (see text), indicating that counting statistics are the dominant source of random error.

during the day and acts to enhance the large topographic contrasts of stationary wave generation with possible differences in large-scale circulation and Walker cell like structures in equatorial regions. We suggest these effects might cause the rapid fluctuations in equatorial and low-latitude data that are measured by the GS.

[13] The general pattern in seasonal Ar concentration is grossly repeated year to year in both the northern and southern hemispheres. The concentration repeatedly peaks in the north at about 4.5% or a factor of 3 greater than the VL2 mass concentration of 1.5%. A statistical test to determine the significance of the north polar winter enhancement was made by S2007, who found a confidence level of 75% for the winter peak of MY 26. The data presented here for MY 27 are of similar S/N and the reader is referred to Figure 11 and related discussion of S2007 if more quantitative information than that we present here regarding the northern winter enhancement is of interest. Enhancement

peaks in the north polar region do not fall at the same L_s in subsequent Mars years. The S/N in the N polar region is inadequate for discovering a particular recurrence of windy season. Measurements made by the NS on Mars Odyssey early in the mission demonstrated noncondensable build up at the north polar region [*Feldman et al.*, 2003] and GRS measurements and analysis were refined enough for S2004 to confirm that Ar enhancement reached the factor of 3. While in southern winter at latitudes above 75°S, concentration increases to 10% or so by midwinter, nearly a factor of 7 enhancement over the VL2 value.

[14] What is new in this paper is that with 3 Mars' years of data, the GS data demonstrate the repeating chaotic nature of the buildup of Ar over the north polar region and its rapid and significant change in abundance on short timescales of 15° increments of L_s which is apparently annual behavior. *Hansen et al.* [2011] elucidate at least one cause of this chaotic behavior in images of slope streaks and small clouds of dust cascading downslopes at 83.5°N, 118.6°E longitude imaged at L_s = 55.7°. Such sediment transport triggered by CO_2 sublimation from leaking of gas trapped beneath the seasonal cap will enhance eddy mixing and the overall fluctuations of Ar enhancement and dilution at high northern latitudes.

[15] In the south polar region, the seasonal Ar concentration exhibits a smoother rise and fall than that in the northern winter (see Figure 1, left, 75°S to 90°S). P2009 computed the seasonal variations in the thickness and distribution of CO_2 ice in the northern and southern hemispheres and modeled a maximum enhancement and seasonal fluctuation for Ar for MYs 26 and 27. A similar behavior for Ar buildup and diminishment to that of the gamma ray data set was discovered. This observation is consistent with the lower mass atmospheric column over the southern highlands, the longer winter and greater CO_2 deposition on the south pole than over the north pole as discussed by S2007. P2009 additionally found that differences in the peak thermal neutron counting rates indicated that there likely was inhibited meridional mixing in MY 26 because of a stronger polar vortex.

[16] Also new in this paper is the advantage of 3 consecutive years of Ar measurement. The amount of entrained Ar brought to winter northern high latitudes by movement of the CO_2 to the polar region is just that expected from the thickness and extent of the seasonal cap. However, because the Ar buildup is chaotic and does not remain close to the factor of 3 enrichment in the North, some Ar may be transported south and cause the southern summer enhancements seen in MY 27 and MY 28 for L_s = 240° to 360° (Figure 1a, left). Other periods of relatively high and low concentration occur near (but not exactly) in time from 1 Mars' year to the next. An interesting and potentially diagnostic feature is a peak at or before L_s = 42° followed by a low at or near at L_s = 60° for all 3 years while Ar is accumulating/mixing in/out of high southern latitudes during autumn (Figure 1a, left). Apparently this period of late autumn in the south experiences turbulence and mixing of frigid air toward lower latitudes. Peak Ar abundance is found in late autumn and early winter for 60°S to 90°S for all three MY but with a slight shift to later season for the 60°S to 75°S zonal bin (Figure 1a, left, and 1b, left).

[17] As suggested by S2004, the south polar vortex must have coherency during long portions of autumn and winter. Insight into the strength and seasonal variation of the southern vortex can be inferred from interannual changes between the summer behavior of the seasonal and residual south polar caps of Mars in MY 28 and 29 in high spatial resolution (pixel scales of 1 km, 5 m, and 0.25 m) images from Mars Reconnaissance Orbiter (MRO) [*James et al.*, 2010] and detailed analysis of curvilinear atmospheric features over Mars' southern hemisphere by *Wang et al.* [2011]. More is discussed about this in section 3.3.

[18] *M. D. Smith et al.* [2001] describe seasonal variations that seem to be in agreement with the CO abundance map retrieved by *Smith et al.* [2009, Figures 10 and 11], with typically a maximum of noncondensable gases around L_s = 120° to L_s = 180° in the latitude range [0°S to 60°S] (note that *Smith et al.* [2009] attribute their other CO maximum around L_s = 300° to an observational artifact due to a dust storm).

[19] Ar data are averaged from 15°S to 15°N and plotted in Figure 2a along with values for a grand average mass mixing ratio of 0.016 (black circle with checked infill on left of Figure 2a) . Data hover around the VL2 measurement shown as a horizontal black line at 0.0145, and exhibit no seasonal trends that ought to be present as the total volume of the atmosphere changes throughout the Martian year. In contrast, in situ measurements of atmospheric Ar made by APXS on both rovers on the MER missions [*Economou*, 2008; *Economou et al.*, 2008] show seasonal changes in Ar concentration. The Ar was measured at the two landing sites of Spirit and Opportunity [*Arvidson et al.*, 2011]. They used the unique capabilities of the APXS to detect the Ar characteristic fluorescent X-ray line at 2950 eV resulting from the bombardment of the atmosphere with alpha particles. At the beginning of the MER missions the APXS was exclusively used to obtain the elemental composition of the Martian samples. However, later in the mission, it was realized that the APXS could also provide additional information on the Martian atmosphere, if the instrument is pointed toward the atmosphere instead of placing it on sample targets. Measurements dedicated to systematic atmospheric Ar measurements were performed with both rovers but we show only results from MER B, Opportunity, in this paper. Figure 2b shows the relative changes in Ar counts per second scaled by an arbitrary constant for comparison to a Mars atmospheric pressure curve (VL 1) for the same seasons. The measured Ar signal follows the same cycle of variation of the Martian pressure but it is not in phase with it. There is an offset of about 50° of L_s between the maximum of the Ar/CO_2 ratio and the Martian pressure maximum. This is interpreted by *Economou* [2008] to illustrate the cyclical phenomenon: at the beginning of spring on a pole the CO_2 ice starts to evaporate, it creates an atmospheric high that forces the air mass from the poles toward the equator where it is observed by Opportunity. The first wave of this air mass that reaches the Opportunity site is very much enhanced in Ar. Subsequent waves continue to increase the atmospheric pressure at the equatorial site, but the Ar amount has already reached the maximum and is continually decreasing, since it was diluted by the constantly evaporating CO_2. The resulting effect is an offset of mixing ratio over the CO_2 pressure of almost two seasons.

[20] APXS measures variation in Ar content close to the ground in equatorial regions with a sensitivity that exceeds that of the orbital GRS measurements. The APXS provides

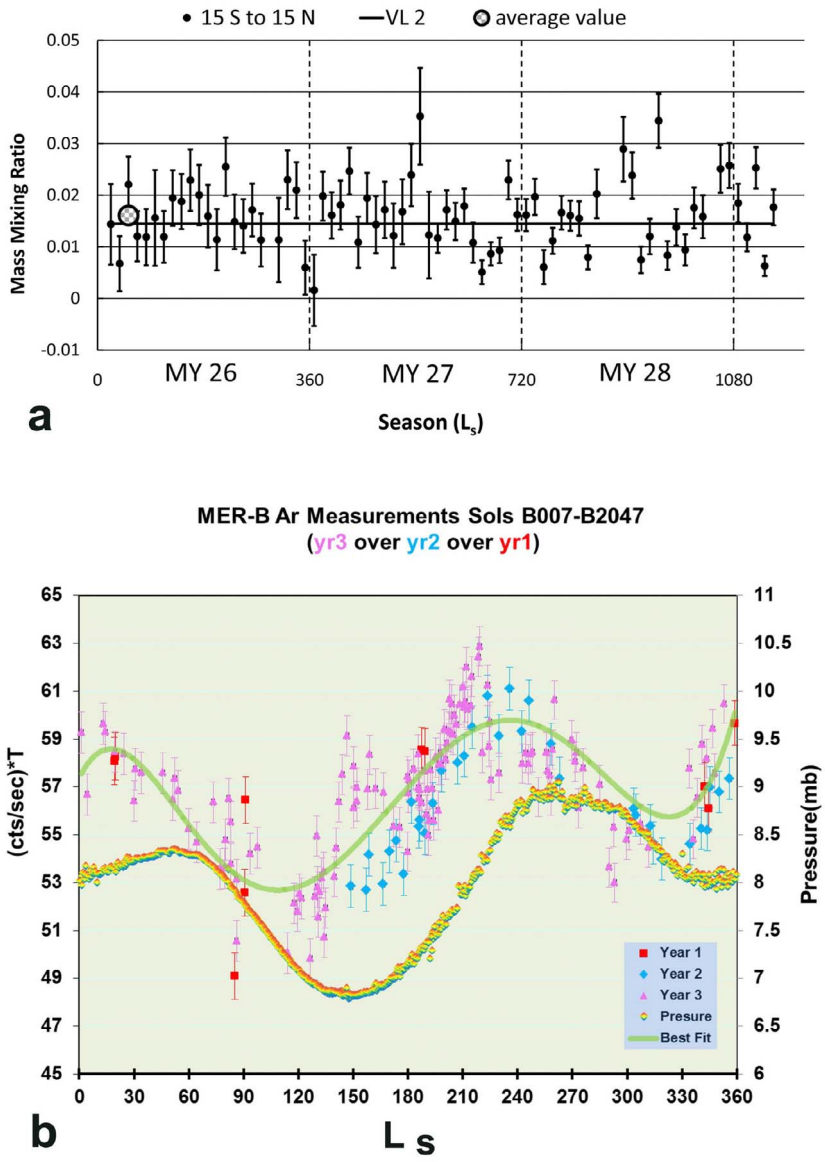

Figure 2. (a) Ar measurements averaged from 15°S to 15°N exhibit no seasonal changes over the 3 year period. The grand average Ar mass mixing ratio (black circle with checked gray interior) falls on and slightly above the Viking 2 value of 0.0145. (b) APXS data exhibit seasonal changes similar for 3 years of measurement. Absolute mixing ratios are not provided, but trends in data are shown by scaling data with an arbitrary constant for easy comparison to an atmospheric pressure curve for the location of the MER B rover (scale on the right-hand side ordinate).

Ar data that can be used to more tightly constrain the processes of Mars GCMs in their efforts discover Mars' seasonal circulation. This is an important result and it is a significant contribution to the GCM groups that are trying to model the short-term and seasonal variations of Mars' atmosphere.

3.2. Evidence for Rapid Mixing Over Long Distances: Selected Region 10° L_s Increments

[21] The episodic nature of Ar enhancement in the north polar region was discussed by S2007. Because the north polar vortex was thought to be coherent and effective in sequestering polar air, the episodic buildup of Ar to its "winter enhanced value" and then rapid decrease to the VL2 concentration on timescales of 30° of L_s was a surprise. This chaotic structure is not consistent with a well controlled coherent polar vortex in the north and more atmospheric modeling has had to account for the sporadic breakup of confining air parcels. Evidence for meridional mixing from northern high latitudes to southern latitudes on short seasonal time scales during southern summer was mentioned in paragraph 16. Evidence for N-S mixing in southern spring (northern autumn) was also observed in MY 27. Figure 3 shows a peak enhancement of Ar concentration in the south to a concentration of 5.9% ± 1.0% that can only be explained by transport from the north. The peak forms and dissipates in 30° of L_s. To test the veracity of this enhancement first observed in the zonal average in 15° increments of L_s (Figure 3, top) we rebinned the same zonal average in 10°

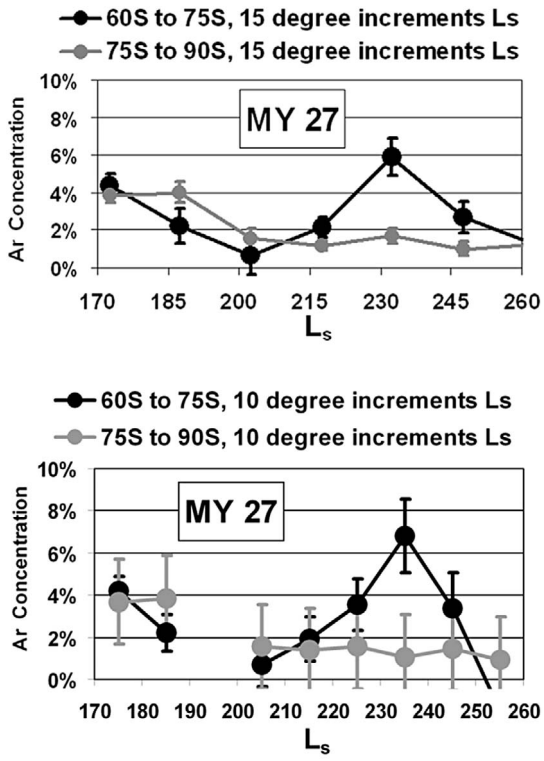

Figure 3. An Ar peak at 60°S to 75°S latitude occurs during northern late autumn. (top) The peak at L_s = 235° was first observed in the normal zonal averages in the seasonal increment of 15° L_s. (bottom) Data are rebinned on a 10° L_s increment which results in a slightly higher Ar concentration at L_s = 235° (see text for discussion).

increments of L_s to examine the rise and fall of Ar concentration with greater time resolution (Figure 3, bottom). The corresponding low point in the 60°N to 75°N Ar data can be seen in Figure 1b (right), gold times data point at L_s = 230° (indicated by gold arrow in Figure 1b, right). This Ar concentration, 0.6% ± 0.3%, is 3-sigma below the mean of the four other points between L_s 195° to 270°, 1.5% ± 0.3%. Another view of the high concentration point in the south is seen in Figure 1b (left), at L_s 230°, gold data points (and gold arrow in Figure 1b, left). This newly discovered evidence for mixing over large distances on short timescales provides a challenge for modeling to understand the driving forces that control the chaotic nature of mixing in the north. In fact, recent modeling by *McConnochie* [2011] shows dramatic wave breaking in the vicinity of the northern Martian polar vortex, and *Malin et al.* [2001] produced ample observations of an active surface reservoir of solid CO_2 which would alter Ar concentration as seen by the GS.

[22] Additional observations which indicate chaotic behavior is to be expected in the atmosphere at high northern latitudes was seen between 28 February 1999 and 25 May 2001, when *D. E. Smith et al.* [2001] observed seasonal changes in the depth of CO_2 frost over northern and southern hemispheres for slightly more than a full Mars year (MYs 24 and 25). Maximum elevations in high latitudes occurred in late winter in both hemispheres. From the temporal changes in patterns of elevations they tracked the seasonal behavior of CO_2 exchange. One result, highlighted here because of its relevancy to the GS Ar data set is that high northern latitudes began to accumulate CO_2 in greater amounts at progressively higher latitudes until L_s = 225° to L_s = 245° when the surface underwent rapid sublimation of up to 30 cm of material. This unpredicted period of CO_2 loss from the surface into the atmosphere correlated with the occurrence of several regional dust storms, mostly in the southern hemisphere that raised the temperature of the atmosphere at midlatitudes to high latitudes in the northern hemisphere by > 20 K [*M. D. Smith et al.*, 2001]. But *D. E. Smith et al.* [2001] point out that the sublimation observed could not be caused by the observed atmospheric heating alone and suggest that redistribution of surface frost by wind may have contributed to the off-season elevation decrease. This would not add to the direct dilution of Ar in the northern high-latitude atmosphere but such windy weather, capable of redistributing ground frost would mix Ar out of the polar highlands to lower latitudes. We point out that this turbulence will contribute to the chaotic nature of the northern winter Ar concentration.

3.3. Mars' Atmospheric Ar in Four Topographically Different Equally Sized Longitude Sectors

[23] In this section we explore the effect of extremes in topography on the distribution of Ar and its seasonal changes. Two years, MY 26 and MY 27, of Mars' atmospheric Ar measurements are used to study annual and seasonal variations in atmospheric transport and mixing in four distinct 90° longitude sectors with different topography (Figure 4). The third year of data (MY 28) has lower S/N and we chose to exclude it from the detailed analysis (see Figure 1).

3.3.1. Effects of Topography: Elysium, Tharsis, Noachis Terra, Hellas

[24] *Encrenaz et al.* [2006], in detailed CO observations with OMEGA on Mars Express, have determined that Hellas basin drives meteorological phenomena. In particular, they found a suggestion of increased CO over Hellas at the end of southern summer. CO, like Ar, is a good tracer for atmospheric circulation. *Forget et al.* [2008] performed GCM modeling of the Hellas region, and an up to a factor of 2 increase in Ar was predicted. Based on these and other suggestions that topography may profoundly affect Mars' atmospheric circulation, we sought to determine the degree to which the Ar gamma ray measurements could be used to explore meteorological changes in Mars' seasonal and local atmospheric behavior.

3.3.2. Influence of Topography on Ar Concentration

[25] The first step was to sum the data within four different longitude sectors, each 90° of longitude. The central longitude of each sector was chosen to coincide with a distinct topographic feature that might drive differences in meridional mixing or seasonal differences in Ar abundance. The four topographic sectors are shown in Figure 4 where atmospheric column abundance in g/cm^2 for L_s = 351° serves as a proxy for surface altitude and topography (Figure 4, left). Profiles of elevation for latitude bins were generated at the spatial resolution of the GRS footprint over the surface of Mars to illustrate the spatial and elevation resolution of the GRS footprint for this study (Figure 4, right).

[26] The S/N in the longitude sector data is consistently good for both MY 26 and 27. However, the interruptions in data collection owing to the spacecraft going into safe mode

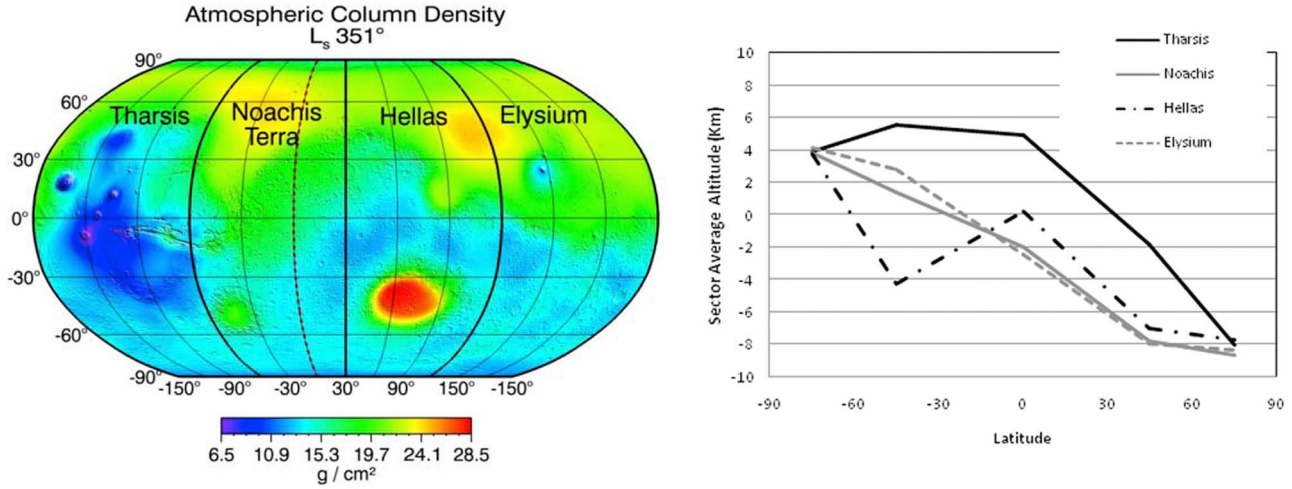

Figure 4. (left) Atmospheric column density proxies for altitude in the map of the four longitude sectors used in this study. Low column densities occur over high terrain and vice versa. (right) Altitude averaged as a function of latitude bin and longitude sector for the four sectors in this study.

early in MY 28, caused changes in the spectral resolution that decreased the S/N in the peak-fitting process. One result is greater scatter in the data and correspondingly larger error bars. These aspects of the data can be seen in Figure 5 which illustrates the seasonal behavior of Ar enrichment for MYs 26, 27, and 28 for the southern high latitude. Within the south polar region where Ar concentration and S/N are high compared to other latitude regions, apparent differences are present but are not easily quantified. Other interesting latitude sectors are those of 30°N to 60°N and 30°S to 60°S where transport out of the polar regions can be seen on a seasonal basis and occasional sporadic enhancements and depletions appear as the perimeter of the ice cap undergoes periodic freezing and subliming (Figures 6a and 6b). The irregular shape of the seasonal cap perimeter experiencing its "crocus date" (date at which subliming begins at the seasonal cap edge) also causes fluctuations that cannot be seen in the zonal averages but can be seen in the 90° longitude bands. Figure 6 illustrates this concept. Note that at this latitude the data accentuate meteorological behavior around Hellas Basin. Our data show that the Hellas sector maintains an Ar enhancement during southern winter at lower latitudes than the other sectors in MY 27. In addition it appears that MY 27 summer Ar is higher in concentration in the Hellas sector than other sectors. This is consistent with the results for CO modeling of *Forget et al.* [2008]. However, the same effect is not seen in the MY 26 late summer. We note that the S/N cannot rule out statistical fluctuations for the effect in MY 28.

3.3.3. Average Winter and Summer Differences in Argon Concentration

[27] Significant differences in the summer and winter Ar abundances have been discovered in the different longitude sectors. Figure 7 shows late autumn and winter concentrations for 30° latitude bins for MY 26 (Figure 7, left) and MY 27 (Figure 7, right). The VL2 value is shown as a hatched black straight line. From top to bottom, Tharsis, Noachis, Hellas, and Elysium sectors are shown. Differences from sector to sector are present, some exceeding 3σ. Differences from year to year are more pronounced yet retain the same

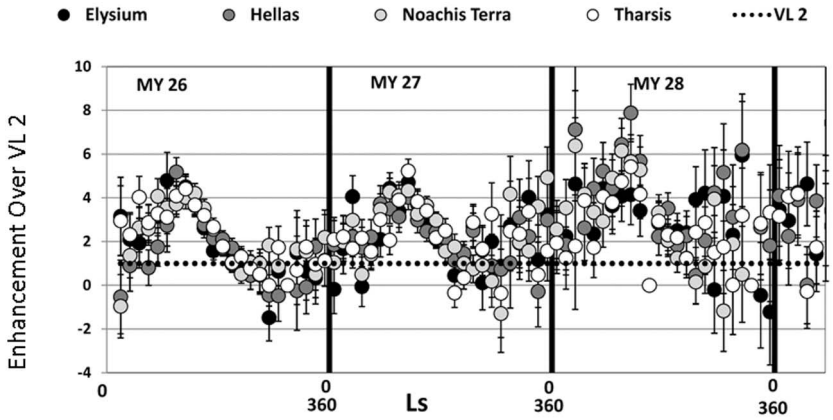

Figure 5. South polar Ar concentrations for the four topographic sectors as a function of 15° increments in L_s. GS sensitivity remained relatively constant throughout MY 27 and the first part of MY 28. The data in MYs 28 and 29 show more scatter following an anneal of the Ge crystal in the gamma sensor head.

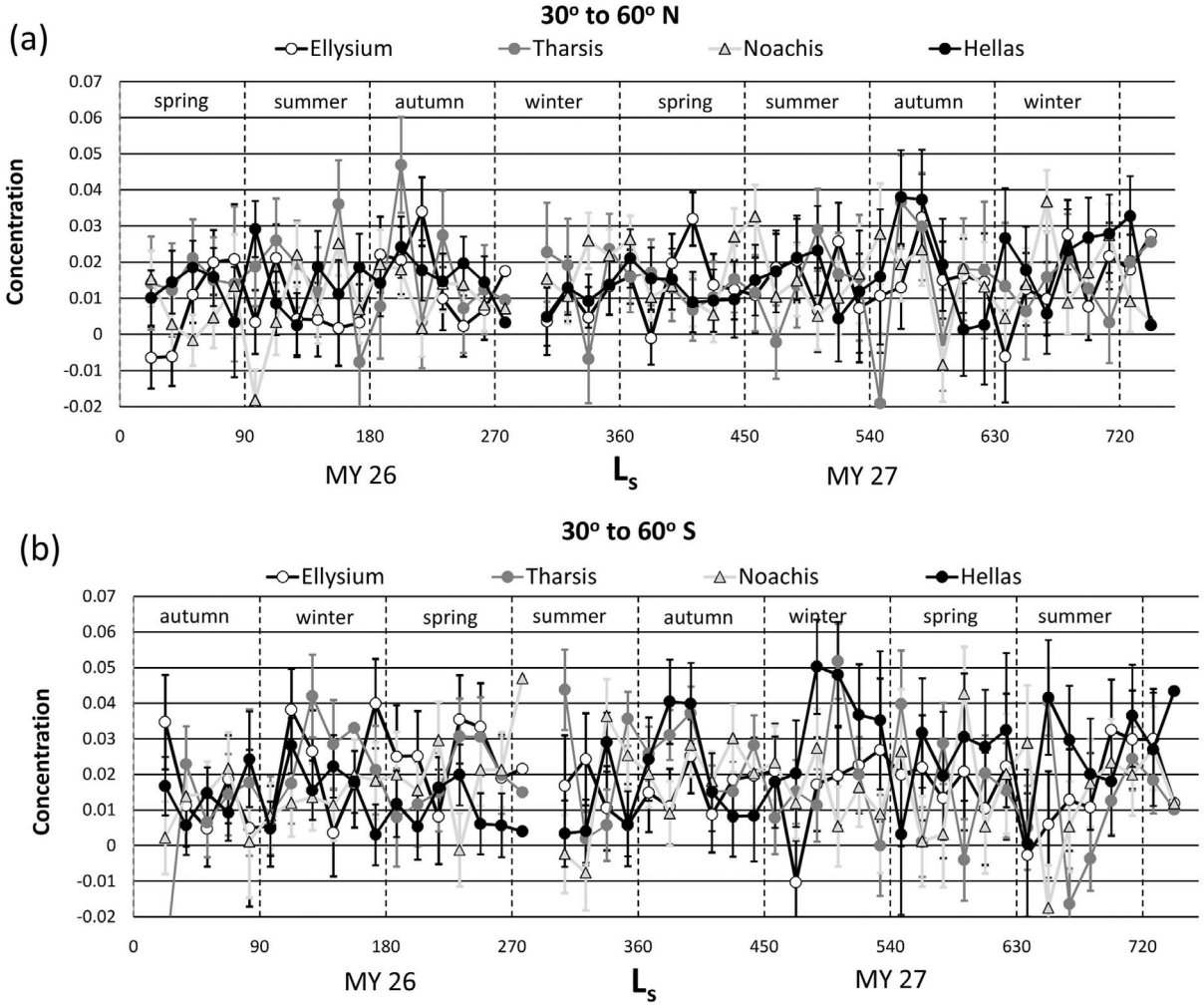

Figure 6. (a) The 30°N to 60°N latitude bin for four geographic sectors during MY 26 and MY 27. (b) Same as Figure 6a but for 30°S to 60°S.

general behavior. Our interpretation is that there is simply slightly different weather in the longitude zones and that weather varies from year to year.

4. Uncertainties and Limitations in the Odyssey Gamma Ray Data Set and Its Analysis

[28] S2004 and S2007 describe in detail their calibration methods and the method of computation of the Ar enhancement factors and Ar concentrations in mass mixing ratio. We refer the reader to those papers for clarification but point out that the calibration uncertainty is estimated to be ~10%. Because we are interested in changes in Ar concentration that are significant at the 2 to 4 sigma level, it is important to show that our estimate of the magnitude of the uncertainties is correct. To test our calculation of uncertainties, we calculated a weighted mean for the low latitudes in MY 26. We found reduced chi squared values of 0.86 for 0°–45°N and 0.90 for 0°–45°S showing that our uncertainties are entirely consistent with the scatter in the data. As a further test of the quality of the data, we calculated a mass balance for each time period by summing all of the latitude bands for MY 26 and 27. We found that except for two of the 46 points the calculated total mass was identical within statistical uncertainties (reduced chi square = 0.87). The two points were at MY 27, L_s = 278° and 308°, and those two time periods are not of any special interest for this work. The data from MY 28 are not as high quality as the earlier data due to radiation damage to the detector that was manifested following a spacecraft safe mode transition where the detector was warmed.

[29] The most important limitation of the GS data set is the need to average over large regions to obtain a S/N that permits discrimination of Ar abundance as a function of season and latitude. In spite of this, S2007 compared the kg/km^2 Ar for the 75°S to 90°S and 60°S to 90°S latitude bands for the "bright" and "dark" regions of the southern polar region as defined by *Kieffer et al.* [2000]. The only statistically significant difference between the concentration of Ar between the "bright" and "dark" regions occurred at MY 26 during L_s = 262.5°, where the bright region had a higher concentration of Ar than the dark region for a brief period in late spring. *Kieffer et al.* point out that the crocus date is earlier for the dark, cryptic region (L_s = 265°) than for the bright terrain (L_s = 275°). S2007 concluded that this divergence in Ar concentration at L_s = 262.5° and subsequent convergence of the values at L_s = 277.5° could be a resonance with the

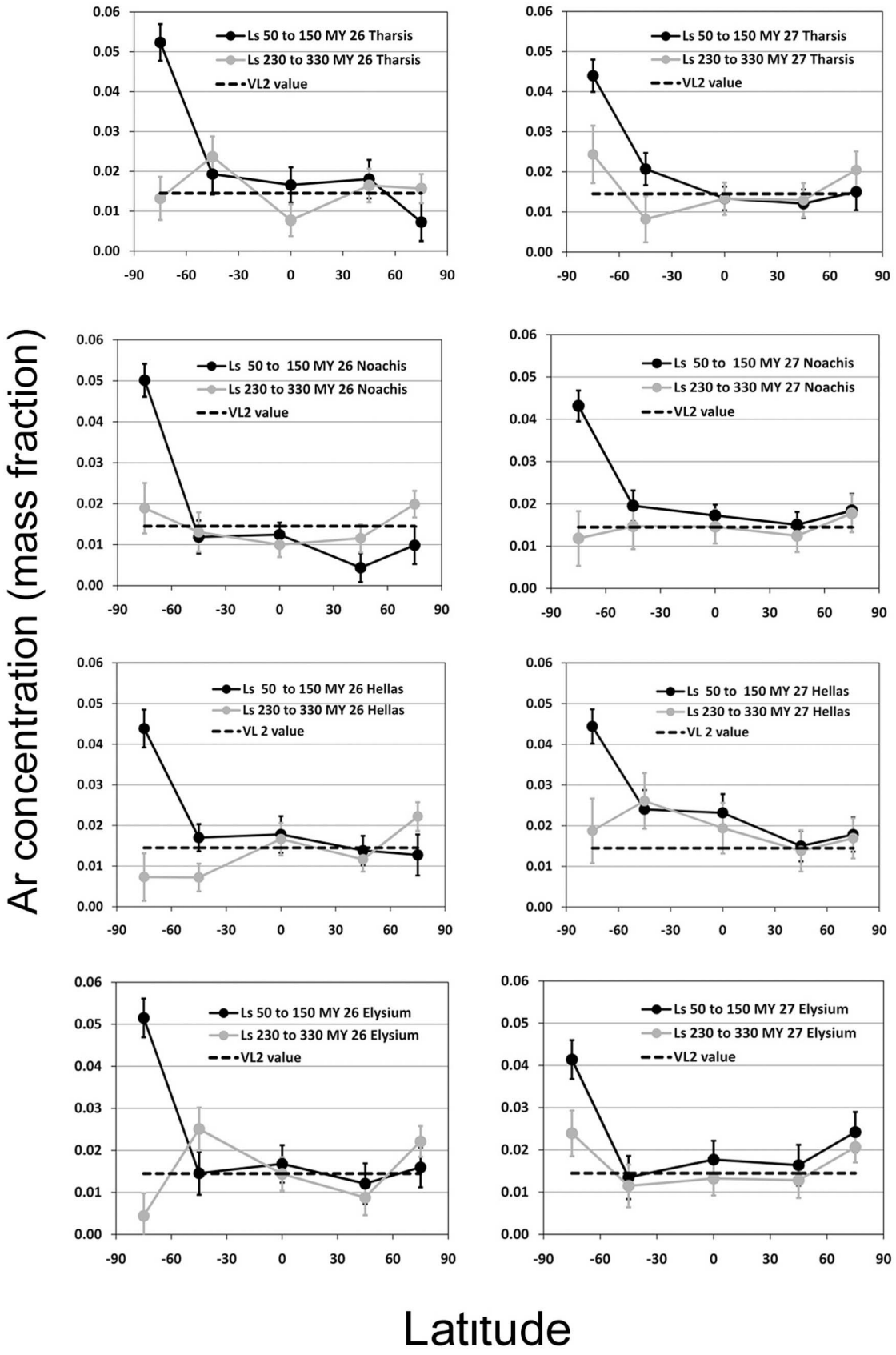
Ar concentration (mass fraction)
Latitude
Ls 50 to 150 MY 26 Tharsis
Ls 230 to 330 MY 26 Tharsis
VL2 value
Ls 50 to 150 MY 27 Tharsis
Ls 230 to 330 MY 27 Tharsis
VL2 value
Ls 50 to 150 MY 26 Noachis
Ls 230 to 330 MY 26 Noachis
VL2 value
Ls 50 to 150 MY 27 Noachis
Ls 230 to 330 MY 27 Noachis
VL2 value
Ls 50 to 150 MY 26 Hellas
Ls 230 to 330 MY 26 Hellas
VL 2 value
Ls 50 to 150 MY 27 Hellas
Ls 230 to 330 MY 27 Hellas
VL 2 value
Ls 50 to 150 MY 26 Elysium
Ls 230 to 330 MY 26 Elysium
VL2 value
Ls 50 to 150 MY 27 Elysium
Ls 230 to 330 MY 27 Elysium
VL2 value

Figure 7

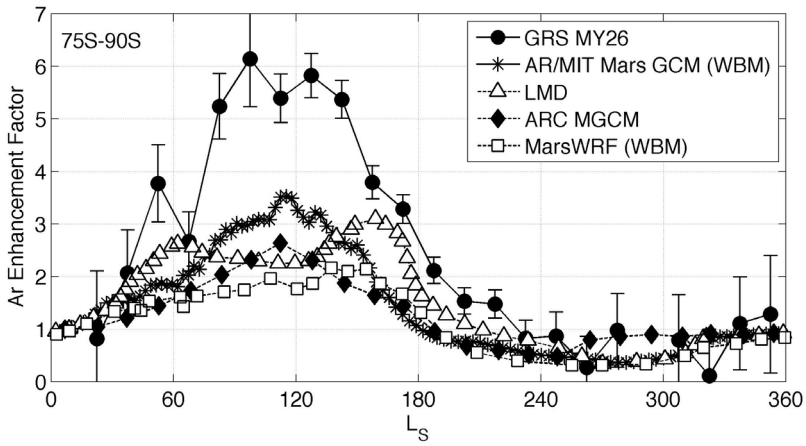

Figure 8. GCM models of high-latitude southern winter compared to gamma ray data for MY 26 (solid black circles with error bars). All models have been scaled to exhibit the same definition of "enhancement factor" as that defined in S2004, S2007 and this paper. See text for details.

subliming CO_2; it sublimes first in the dark terrain, diluting the Ar concentration while the concentration remains high in the bright terrain. Also, as discussed in sections 3.2 and 3.3, some geographic and seasonal discrimination has been successful with slightly altered binning schemes (10° increments in L_s, 90° longitude sectors).

[30] Our models, here and in previous papers use standard atmospheres, as discussed in paragraph 9, with no account taken for the evolution of the convective boundary layer height. Martian mesoscale/microscale winds and surface energy effects can warm and raise the atmospheric mass. *Spiga et al.* [2011] show that mixing layer depths in various geographical locations will be affected and large changes in the magnitude of eddy mixing results. In our analysis of the Ar data we assume Ar is distributed according to mass mixing ratio along the entire column of gas in the first scale height. These approximations introduce only a small systematic uncertainty in our enhancement factors for the spatial and temporal Ar analysis. The thermal neutron excitation flux of the Ar is greater closer to the ground, but the transmission of the gamma rays through the upper atmosphere is less. For example, if all of the Ar were concentrated in the bottom 25% of the atmosphere, the gamma flux would increase by only 13% relative to the case of homogeneous distribution. The APXS measurements did see significant seasonal changes in equatorial Ar concentration in data obtained closer to the ground.

5. The GRS Data Set as a Standard for Mars Global Circulation Models

[31] We are in an exciting period of Mars exploration simultaneously using in situ measurement, orbital remote sensing, and sophisticated atmospheric modeling in an effort to discern the past, present, and future Mars weather and climate. Mars atmospheric Ar measurements are of interest to planetary scientists, particularly those modeling its atmosphere, because knowing the seasonal and global distribution of Ar both provides quantitative constraints on wind vector fields and other transport parameters for Mars GCMs [cf. *Colaprete et al.*, 2008; *Forget et al.*, 1999; *Haberle et al.*, 1999]. These predictions are critical to understanding the conditions at Mars that have existed over its history and were, or are, conducive to the origin and sustenance of living organisms. Despite four different GCM studies of the GS Ar data, the observations remain a major challenge to models of atmospheric transport. The NASA Ames, LMD, and MarsWRF GCM models all produce southern polar enhancement factor magnitudes that are 2–3 times too small compared to observations (if compared using a common definition of enhancement factor). Figure 8 illustrates this point with plots of the southern winter enhancement factors of the four published model results along with the GS data from S2004. Using a more advanced finite volume, cubed sphere GCM with second-order moment transport, the AR/MIT Mars GCM can simulate a peak enhancement factor of 4.5 (not shown) versus the 6 observed. Clearly the Ar observations remain a major challenge for modeling Martian atmospheric transport.

[32] One area in which the GS Ar data have profoundly influenced this process is to reveal the limitations of the world's most prestigious GCMs to predict seasonal meridional transport. *Nelli et al.* [2007] made a detailed study of the NASA ARC GCM by extensive modeling of Ar transport in an experiment in which major parameters (elipticity, albedo, topography, emissivity) were tested to determine their influence on Ar seasonal concentration. The best models underestimated the peak Ar concentration by a factor of 2 at both

Figure 7. GS Ar data binned 30° in latitude and 90° in longitude for the four geologic sectors discussed and shown in Figure 4 for (left) MY 26 and (right) MY 27. Black lines and points are (L_s = 50° to L_s = 150°) averages of partial autumn/winter for southern latitudes and partial spring/summer for northern latitudes. Gray lines and points are (L_s = 230° to L_s = 330°) averages of partial spring/summer for southern latitudes and partial autumn/winter for northern latitudes. VL2 Ar concentration is shown as dashed black horizontal line. For discussion, see text.

polar regions. However, they did get the correct sense of enhancement–that is more in southern winter than in northern winter. *Guo et al.* [2007] used the Mars PlanetWRF General circulation model to simulate the cycle of noncondensable gases and obtained results analogous to those of *Nelli et al.* [2007], with appropriate seasonal variations (more noncondensables at high latitudes during winter), but very weak enhancement in Ar compared to the observations in the southern hemisphere. Using the LMD Mars GCM, *Forget et al.* [2008] performed similar simulations, although unlike the previous two studies they included a detailed scheme to simulate the variation of Ar and N_2 mixing ratio in the vertical, taking into account the convective motions induced by the vertical gradient in air molecular mass. *Forget et al.* [2009] report enhancement of roughly 3 in polar night over the south pole but argue that the GRS observation calibration against Viking Lander 2 may be incorrect. On this basis, they show plots that are scaled to match the peak Ar abundances observed [*Forget et al.*, 2009, Figure 1; *Lefèvre and Forget*, 2009, Supplementary Material].

[33] The underestimation of the enhancement factor during southern winter by most models can result from many factors. On the one hand models may not well represent the complex meteorological processes occurring in the polar night, and as a results underestimate the strength of the southern polar vortex. For instance, *Colaprete et al.* [2008] significantly altered the NASA ARC GCM adding many new microphysical parameters and convection from condensation available potential energy (CAPE). The amount and character of noncondensable transport was improved with predicted abundances and distribution somewhat improved. Another factor of interest is that the GCM numerical scheme used to compute the transport may be incorrect (for instance because of their numerics, their limited resolution, etc.), and, as a result overestimate transport and diffusion compared to reality. This was recently explored by *Lian et al.* [2012], who used the PlanetWRF Mars physical package [*Richardson et al.* 2007] coupled with the state of the art MIT GCM dynamical core based on cube-sphere grid finite volume numerics and which has several options for the tracer advection scheme. They found significant variations depending on the quality of the schemes used and suggested that much (but probably not all) of the variations between different prior modeling studies as well as the differences with the data is plausibly related to differences in the advection schemes used. They conclude that improvements in transport representation, the quality of the simulation of atmospheric circulation, and the completeness of treatment of physical processes related to CO_2 condensation are likely necessary before models can credibly simulate the Ar enhancement factor variations at the southern pole.

6. Summary and Conclusions

[34] The gamma ray spectrometer on board Mars Odyssey spacecraft has provided a data set of Mars' atmospheric Ar that has profoundly changed our view of the planet's atmospheric circulation. Strong seasonal variations at southern polar latitude show the southern vortex must be coherent and strong in late autumn and early winter. In contrast, the northern vortex must be weaker by comparison of the effectiveness of sequestering Ar throughout polar night. At the spatial scales resolved by the GS, Mars atmospheric transport and weather is grossly similar from year to year but punctuated by turbulence and occasional rapid meridional transport. For the purposes of modeling the atmosphere, the high Ar concentrations during late autumn and winter seasons serve as a standard for testing Mars GCM, a standard the models cannot currently satisfy. The Ar data provide a stern test of Mars GCMs at arguably the most challenging time and location for models, the tightly confined core of the highly isolating southern polar vortex. It is then perhaps not surprising the models struggle with the southern polar Ar observations, but it seems equally clear that confidence in other, more complex transport-dependent systems, like the water and dust cycles, requires models first adequately simulate the much simpler Ar cycle.

[35] **Acknowledgments.** We acknowledge the contributions of the entire GRS team, Bob Haberle for providing great discussion and the NASA ARC MGCM output 2002.17 for analysis purposes, and funding from NASA contract 1228726. Mike Finch provided the topographic computations and maps, and Kris Kelly provided the initial summing of Ar data used by S2004 and S2007. In addition, we thank two reviewers who kindly helped to improve this paper.

References

Arvidson, R. E., et al. (2011), Opportunity Mars Rover mission: Overview and selected results from Purgatory ripple to traverses to Endeavour crater, *J. Geophys. Res.*, *116*, E00F15, doi:10.1029/2010JE003746.

Billebaud, F., et al. (2009), Observations of CO in the atmosphere of Mars with PFS onboard Mars Express, *Planet. Space Sci.*, *57*(12), 1446–1457, doi:10.1016/j.pss.2009.07.004.

Boynton, W. V., et al. (2004), The Mars Odyssey Gamma-Ray Spectrometer instrument suite, *Space Sci. Rev.*, *110*, 37–83, doi:10.1023/B:SPAC.0000021007.76126.15.

Colaprete, A., R. M. Haberle, and O. B. Toon (2003), Formation of convective carbon dioxide clouds near the south pole of Mars, *J. Geophys. Res.*, *108*(E7), 5081, doi:10.1029/2003JE002053.

Colaprete, A., J. R. Barnes, R. M. Haberle, and F. Montmessin (2008), CO_2 clouds, CAPE and convection on Mars: Observations and general circulation modeling, *Planet. Space Sci.*, *56*(2), 150–180, doi:10.1016/j.pss.2007.08.010.

Economou, T. E. (2008), Mars atmosphere argon density measurement on MER Mission, paper presented at Third International Workshop on the Mars Atmosphere: Modeling and Observations, Lunar and Planet. Inst., Williamsburg, Va., 10–13 Nov.

Economou, T. E., and R. T. Pierrehumbert (2010), Mars atmosphere argon density measurements on MER missions, *Proc. Lunar Planet. Sci. Conf.*, *41st*, Abstract 2179.

Economou, T. E., R. I. Citron, and R. T. Pierrehumbert (2008), Measurement of Mars atmosphere argon density with the APXS on the Opportunity site, *Eos Trans. AGU*, *89*(53), Fall Meet. Suppl., Abstract P53A-1441.

Encrenaz, T., T. Fouchet, R. Melchiorri, P. Drossart, B. Gondet, Y. Langevin, J.-P. Bibring, F. Forget, and B. Bezard (2006), Seasonal variations of the Martian CO over Hellas as observed by OMEGA/Mars Express, *Astron. Astrophys.*, *459*, 265–270, doi:10.1051/0004-6361:20065586.

Feldman, W. C., et al. (2003), CO_2 frost cap thickness on Mars during northern winter and spring, *J. Geophys. Res.*, *108*(E9), 5103, doi:10.1029/2003JE002101.

Forget, F., F. Hourdin, R. Fournier, C. Hourdin, O. Talagrand, M. Collins, S. R. Lewis, P. L. Read, and J.-P. Huot (1999), Improved general circulation models of the Martian atmosphere from the surface to above 80 km, *J. Geophys. Res.*, *104*, 24,155–24,175, doi:10.1029/1999JE001025.

Forget, F., et al. (2007a), The new (version 4.2) Mars climate database, paper presented at Seventh International Conference on Mars, Lunar and Planet. Inst., Pasadena, Calif., 9–13 July.

Forget, F., A. Spiga, B. Dolla, S. Vinatier, R. Melchiorri, P. Drossart, A. Gendrin, J.-P. Bibring, Y. Langevin, and B. Gondet (2007b), Remote sensing of surface pressure on Mars with the Mars Express/OMEGA spectrometer: 1. Retrieval method, *J. Geophys. Res.*, *112*, E08S15, doi:10.1029/2006JE002871.

Forget, F., E. Millour, L. Montabone, and F. Lefevre (2008), Non condensable gas enrichment and depletion in the Martian polar regions, paper presented at Third International Workshop on the Mars Atmosphere: Modeling and Observations, Lunar and Planet. Inst., Williamsburg, Va., 10–13 Nov.

Forget, F., E. Millour, L. Montabone, and F. Lefevre (2009), Non condensable gas enrichment and depletion in the Martian polar regions, *LPI Contrib.*, *1494*, 15–16.

Guo, X., M. I. Richardson, C. E. Newman, A. L. Sprague, and W. V. Boynton (2007), Non-condensable gas in a Mars general circulation model, *Eos Trans. AGU*, *88*(52), Fall Meet. Suppl., Abstract P11A-0260.

Haberle, R. M., J. B. Pollack, J. R. Barnes, R. W. Zurek, C. B. Leovy, J. R. Murphy, H. Lee, and J. Schaeffer (1993), Mars atmospheric dynamics as simulated by NASA Ames general circulation model: 1. The zonal mean circulation, *J. Geophys. Res.*, *98*, 3093–3123, doi:10.1029/92JE02946.

Haberle, R. M., M. M. Joshi, J. R. Murphy, J. R. Barnes, J. T. Schofield, G. Wilson, M. Lopez-Valverde, J. L. Hollingsworth, A. F. C. Bridger, and J. Schaeffer (1999), General circulation model simulations of the Mars Pathfinder atmospheric structure investigation/meteorology data, *J. Geophys. Res.*, *104*, 8957–8974, doi:10.1029/1998JE900040.

Haberle, R., J. R. Murphy, and J. Schaeffer (2003), Orbital change experiments with a Mars general circulation model, *Icarus*, *161*, 66–89, doi:10.1016/S0019-1035(02)00017-9.

Hansen, C. J., et al. (2011), Seasonal erosion and restoration of Mars' northern polar dunes, *Science*, *331*, 575–578, doi:10.1126/science.1197636.

Hollingsworth, J. L., and J. R. Barnes (1996), Forced stationary planetary waves in Mars's winter atmosphere, *J. Atmos. Sci.*, *53*(3), 428–448, doi:10.1175/1520-0469(1996)053<0428:FSPWIM>2.0.CO;2.

James, P. B., P. C. Thomas, and M. C. Malin (2010), Variability of the south polar cap of Mars in Mars years 28 and 29, *Icarus*, *208*, 82–85, doi:10.1016/j.icarus.2010.02.007.

Kieffer, H. H., T. N. Titus, K. F. Mullins, and P. R. Christensen (2000), Mars south polar spring and summer behavior observed by TES: Seasonal cap evolution controlled by frost grain size, *J. Geophys. Res.*, *105*, 9653–9699, doi:10.1029/1999JE001136.

Krasnopolsky, V. A. (2003), Spectroscopic mapping of Mars CO mixing ratio: Detection of north-south asymmetry, *J. Geophys. Res.*, *108*(E2), 5010, doi:10.1029/2002JE001926.

Lefèvre, F., and F. Forget (2009), Observed variations of methane on Mars unexplained by known atmospheric chemistry and physics, *Nature*, *460*(7256), 720–723, doi:10.1038/nature08228.

Leovy, C., and Y. Mintz (1969), Numerical simulation of the atmospheric circulation and climate of Mars, *J. Atmos. Sci.*, *26*(6), 1167–1190, doi:10.1175/1520-0469(1969)026<1167:NSOTAC>2.0.CO;2.

Lian, Y., M. I. Richardson, C. E. Newman, C. Lee, A. D. Toigo, M. A. Mischna, and J. Campin (2012), The Ashima/MIT Mars GCM and argon in the Martian atmosphere. *Icarus*, *218*, 1043–1070, doi:10.1016/j.icarus.2012.02.012.

Malin, M. C., M. A. Caplinger, and S. D. Davis (2001), Observational evidence for an active surface reservoir of solid carbon dioxide on Mars, *Science*, *294*, 2146–2148, doi:10.1126/science.1066416.

McConnochie, T. H. (2011), Planetary wave breaking and the "surf zone" in the vicinity of the Martian polar vortex, paper presented at the Fourth International Workshop on the Mars Atmosphere: Modelling and Observation, CNES, Paris, 8–11 February.

Murphy, J. R., J. B. Pollack, R. M. Haberle, C. B. Leovy, O. B. Toon, and J. Schaeffer (1995), Three-dimensional numerical simulation of Martian global dust storms, *J. Geophys. Res.*, *100*, 26,357–26,376, doi:10.1029/95JE02984.

Nelli, S. M., J. R. Murphy, A. L. Sprague, W. V. Boynton, K. E. Kerry, D. M. Janes, and A. E. Metzger (2007), Dissecting the polar dichotomy of the noncondensable gas enhancement on Mars using the NASA Ames Mars General Circulation Model, *J. Geophys. Res.*, *112*, E08S91, doi:10.1029/2006JE002849.

Owen, T., K. Biemann, D. R. Rushneck, J. E. Biller, D. W. Howarth, and A. L. Lafleur (1977), The composition of the atmosphere at the surface of Mars, *J. Geophys. Res.*, *82*, 4635–4639, doi:10.1029/JS082i028p04635.

Pollack, J. B., R. M. Haberle, J. Schaeffer, and H. Lee (1990), Simulations of the general circulation of the Martian atmosphere: 1. Polar processes, *J. Geophys. Res.*, *95*, 1447–1473, doi:10.1029/JB095iB02p01447.

Prettyman, T. H., et al. (2004), Composition and structure of the Martian surface at high southern latitudes from neutron spectroscopy, *J. Geophys. Res.*, *109*, E05001, doi:10.1029/2003JE002139.

Prettyman, T. H., W. C. Feldman, and T. N. Titus (2009), Characterization of Mars' seasonal caps using neutron spectroscopy, *J. Geophys. Res.*, *114*, E08005, doi:10.1029/2008JE003275.

Richardson, M. I., A. D. Toigo, and C. E. Newman (2007), PlanetWRF: A general purpose, local to global numerical model for planetary atmospheric and climate dynamics, *J. Geophys. Res.*, *112*, E09001, doi:10.1029/2006JE002825.

Smith, D. E., M. T. Zuber, and G. A. Neumann (2001), Seasonal variations of snow depth on Mars, *Science*, *294*, 2141–2146, doi:10.1126/science.1066556.

Smith, M. D., J. C. Pearl, B. J. Conrath, and P. R. Christensen (2001), One Martian year of atmospheric observations by the Thermal Emission Spectrometer, *Geophys. Res. Lett.*, *28*, 4263–4266, doi:10.1029/2001GL013608.

Smith, M. D., M. J. Wolff, R. T. Clancy, and S. L. Murchie (2009), Compact Reconnaissance Imaging Spectrometer observations of water vapor and carbon monoxide, *J. Geophys. Res.*, *114*, E00D03, doi:10.1029/2008JE003288.

Spiga, A., F. O. Forget, J.-B. Madeleine, L. Montabone, S. R. Lewis, and E. Millour (2011), The impact of Martian mesoscale winds on surface temperature and on the determination of thermal inertia, *Icarus*, *212*, 504–519, doi:10.1016/j.icarus.2011.02.001.

Sprague, A. L., W. V. Boynton, K. E. Kerry, D. M. Janes, D. M. Hunten, K. J. Kim, R. C. Reedy, and A. E. Metzger (2004), Mars' south polar Ar enhancement: A tracer for south polar seasonal meridional mixing, *Science*, *306*, 1364–1367, doi:10.1126/science.1098496.

Sprague, A. L., W. V. Boynton, K. E. Kerry, D. M. Janes, N. J. Kelly, M. K. Crombie, S. M. Nelli, J. R. Murphy, R. C. Reedy, and A. E. Metzger (2007), Mars' atmospheric argon: Tracer for understanding Martian atmospheric circulation and dynamics, *J. Geophys. Res.*, *112*, E03S02, doi:10.1029/2005JE002597.

Suarez, M. J., and L. L. Takacs (1995), Documentation of the AIRES/GEOS dynamical core version 2, *NASA Tech. Memo.*, *TM-104606*, 45 pp.

Wang, H., A. D. Toigo, and M. I. Richardson (2011), Curvilinear features in the southern hemisphere observed by Mars Global Surveyor Mars Orbiter Camera, *Icarus*, *215*, 242–252, doi:10.1016/j.icarus.2011.06.029.

Waters, L. S. (1999), MCNPX user's guide, *Rep. LA-UR-99*, Los Alamos Natl. Lab., Los Alamos, N. M.

W. V. Boynton, D. Hamara, and A. L. Sprague, Lunar and Planetary Laboratory, University of Arizona, 1629 E. University Blvd., Tucson, AZ 85721, USA. (sprague@lpl.arizona.edu)

T. Economou, Laboratory for Astrophysics and Space Research, University of Chicago, 933 E. 56th St., Chicago, IL 60637, USA.

F. Forget, Laboratoire de Météorologie Dynamique, CNRS, Université Pierre et Marie Curie, 4, pl. Jussieu, F-75005 Paris CEDEX 05, France.

Y. Lian and M. Richardson, Ashima Research, 600 S. Lake Ave., Ste. 104, Pasadena, CA 91106, USA.

A. E. Metzger, Jet Propulsion Laboratory, 4800 Oak Grove Dr., Pasadena, CA 91109, USA.

R. Starr, Department of Physics, Catholic University, 620 Michigan Ave. NE, Washington, DC, 20064, USA.